Inkjet printing of adamantane-type organotin sulfide clusters featuring extreme nonlinear optical properties

Check for updates

Simon Nier[1], Yannick R. Lohse [1], Niklas Rinn[1], Gabriel Cadilha Marques [1], Nils W. Rosemann [2], Marius Welzel [3], Dominik Heider [3], Jasmin Aghassi-Hagmann [1] ✉ & Stefanie Dehnen [1] ✉

Inkjet printing has emerged as a powerful technique for manufacturing metals, metal oxides or nanoparticles and is stimulating the research on electronic and data storage devices, light-emitting diodes, and even photovoltaics. Usually, such inks either contain metal salts or nanoparticles. More complex compounds, like hybrid inorganic-organic cluster molecules, would allow for even more versatile and tailor-made properties of the printed materials. However, poor solubility, thermal lability or water sensitivity prohibited inkjet processing of such compounds to date. Here we show that the well-soluble and robust cluster compound $[\{(4\text{-}n\text{-pentyl-phenyl})Sn\}_4S_6]$ (pentyl: C_5H_{11}; phenyl: C_6H_5), of which amorphous bulk material exhibits white-light generation upon infrared-laser diode irradiation. The compound allows formulation into inks for inkjet printing without affecting the clusters' identity and controlled deposition in well-defined micro-structured patterns. Besides the proof-of-principle for printing complex structures with tailor-made optical responses, the deposited material is soluble in common solvents for potential reuse. We envision that these hybrid cluster-based inks will pave the way to printable optical information storage devices.

In the 1970s and 1980s, following the advances of inkjet printing, the first commercially available printers were produced[1]. Since then, a huge variety of different inkjet techniques and inks have been developed, and now play an important role in daily life. Besides the ordinary use as an office inkjet printer, this technology can also be employed as a precise and cost-effective deposition method down to the micron scale for functional materials and devices[1–4]—in addition to laser-printing[5,6] and other digital printing technologies[7]. Different types of inkjet-printed materials have been reported, including metal complexes of silver[8], copper[9], platinum[10–12], gold[13], and iron[14]. Additionally, nanoparticles (NPs) made of Ag[15], Pt[10], SnO$_2$[16], ZnO$_2$[17], Pd[18], or Au[19], as well as Ag-Cu core-shell NPs[20] can also be used in printable inks, which have already found their way into several applications. Examples are inkjet-printed resistive switching devices[21], flexible conductive structures, and printable conductive materials[22]. Many optically active materials consist of quantum dots (QDs), and have been used for the fabrication of QD-based light emitting diodes (QDLEDs)[23] or micro-light-emitting diodes (μLEDs)[24], which are promising candidates for next-generation display technologies. While ordinary NPs can easily be substituted by non-toxic alternatives, the most efficient QDs are composed of toxic metals (e.g., Cd,

Hg, Pb), which are subject to the "Restriction of Hazardous Substances" directive in the European Union. Furthermore, non-toxic alternatives, like InP QDs, show a lack of stability under photoactivation. Due to photo corrosion or thermal degradation processes nearly all QDs without a protecting shell show severe degradation in accelerated aging experiments. Even with such protective layers or ligand modification, many QDs still undergo degradation processes[25]. Therefore, the variety of printable optically active materials without toxic metals, which at the same time are air and moisture stable, have been very rarely described.

Organotetrel chalcogenide clusters offer potential solutions to these issues. They can be divided into different topologies, of which the adamantane-type structure with the general formula $[(RT)_4E_6]$ (R = organic substituent; T = Sn, Ge, Si; E = Te, Se, S) will be in the spotlight of this work. Excitation of these types of clusters with a continuous-wave (CW) infrared laser diode produces an extreme nonlinear optical response. Depending on the (crystalline or amorphous) habitus of the sample and the nature of the organic substituents this manifests itself either as frequency doubling (second harmonic generation, SHG) or the generation of a broad emission covering the whole visible range, i.e., a white-light spectrum (white-light

Fig. 1 | Schematic representation of the ink preparation and printing processes as well as the probing of the resulting printed pattern.
a Synthesis of the adamantane-type cluster compound. **b** Formulation of the ink in different media and loading of a printer cartridge. **c** Test printing on a Dimatix DMP-2850 printer and evaluation of the materials stability after printing via Raman spectroscopy. **d** Optimization of resolution and homogeneity using the Super Inkjet Printer to form well defined patterns resulting in a binary code for eventual optical probing.
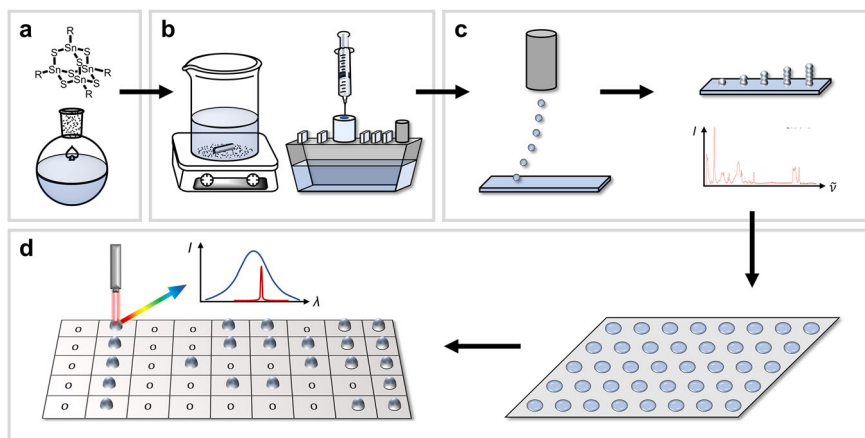
generation, WLG[26–28]. As shown by previous studies, the observation of one effect or the other is largely dependent on the degree of long-range order in the material, which in case of (nano)crystalline samples causes the former based on surface effects, and in the absence of long-range order causes the latter[26,28]. The habitus can be controlled by the elemental composition of the $\{T_4E_6\}$ cluster core and the nature of the organic substituents R[29,30]. Only substituents that provide a high electron density close to the cluster core, which is ideally achieved with phenyl (Ph) groups. Notably, the substituents at the same time control the solubility of the compound, which is instrumental for their utilization in printable inks.

Based on their specific optical responses, such compounds can theoretically be used to 'write' and 'read' binary code in digital data. Inspired by the field of printed electronics, the deposition of the clusters on a suitable material represents the 'writing' process. Inkjet printing as a deposition method is a precise, material-saving and cost-effective deposition technique to create such data storage devices. The 'read' process would be performed using a CW infrared laser diode. Eventually, such data could be integrated into long-term data storage devices, given the high robustness and thermal stability of the clusters.

A major challenge to overcome for a proof of principle is the fact that the majority of white-light-emitting clusters $[(RSn)_4S_6]$ known in the literature are only poorly soluble in common organic solvents or water. The parent compound $[(PhSn)_4S_6]$ (**A**; Ph = phenyl = C_6H_5), for instance, exhibits solubilities of only 50 mg mL^{-1} in tetrahydrofuran (THF) or 20 mg mL^{-1} in toluene. This contradicts the observation of the non-linear optical effects that require more than only a few traces of the material. Typical inkjet printers produce picolitre-sized drops and transfer micro- to nanogram quantities onto the substrates, e.g., on glass slides, Si wafers, or even flexible substrates such as PET foil or Kapton™. It is obvious that higher solubilities are therefore required to transfer reasonable amounts of the cluster compound to the substrate. Other prerequisites for successful printing are connected to the physical properties of the solvent and the resulting ink. Besides a high boiling point for better printability, the surface tension and viscosity of the ink have to be adjusted to the requirements of the printer. The viscosity can be decreased or increased by changing the temperature at the print head or by adding highly viscous additives. The surface tension can be reduced by adding surfactants. Increasing the surface tension is not easily possible, however, which is why using a solvent with a high surface tension is mandatory. High operating temperatures of the print head of up to 70 °C, and contact of the ink with air could, in theory, lead to decomposition of the molecules when printing clusters. Recording of Raman spectra is therefore advisable to check whether the cluster remained intact or not.

Here we show that by design of a corresponding cluster compound we can provide the proof of principle for successful inkjet printing for cluster-based materials, which will be transferable to other related materials. The

strategy was based on the decoration of the clusters with organic substituents that would combine the prerequisite for the white-light generation (hence, a phenyl substituent), with sufficiently high solubility (upon addition of terminal alkyl chains). The final goal of this study, printing a binary string with optimal settings, was finally achieved this way. The fabrication scheme is illustrated in Fig. 1.

Results and discussion
Synthesis, structure, and white-light generation of [{(4-*n*-pentyl-phenyl)Sn}$_4$S$_6$] (1)
Starting from 4-*n*-pentyl-phenyl bromide (pentyl = C_5H_{11}), the adamantane-type cluster compound [{(4-*n*-pentyl-phenyl)Sn}$_4$S$_6$] (**1**) was prepared via a three-step process in a large multigram-scale unusual for such cluster compounds. First, (4-*n*-pentyl-phenyl)$_4$Sn (**I**) was prepared in single-crystalline form from the appropriate Grignard compound and SnCl$_4$ (37.34 g, 68% yield). Following a Kocheshkov redistribution reaction with further SnCl$_4$, (4-*n*-pentyl-phenyl)SnCl$_3$ (**II**, 3.13 g, 74% yield) was isolated and subsequently converted to compound **1** by reaction with (Me$_3$Si)$_2$S (8.62 g, 92% yield). Supplementary Figs. 1–11 show nuclear magnetic resonance (NMR) spectra of compounds **I** and **1**, Supplementary Fig. 12 and 13 show infrared (IR) spectra of compounds **I** and **1**. Compound **1** crystallizes in the triclinic crystal system, space group type $P\bar{1}$, with the expected adamantane-type $\{Sn_4S_6\}$ structural motif. Supplementary Tables 1–4 provide details of the X-ray diffraction experiments, refinements, and selected structural parameters; Supplementary Figs. 14 and 15 show structural diagrams with the full atom labelling scheme. The S–Sn bond lengths ranging between 2.382(1) and 2.412(1) Å, consistent with previously reported structures of $[(BnSn)_4S_6]$ (Bn = benzyl, C_6H_5-CH$_2$)[31], [Au(dppe)$_2$] $[(RSn)_4S_6Cl]$ (dppe = Ph$_2$PC$_2$H$_4$PPh$_2$; R = C(CH$_3$)$_2$CH$_2$C(CH$_3$)NNH$_2$)[32], and $[(FcSn)_4S_6]$ (Fc = Fe(C$_5$H$_5$)$_2$)[33]. The molecular structure of **1** and the packing scheme of the molecules in the crystal are shown in Fig. 2.

Due to the crystallization of compound **1** in the centrosymmetric space group $P\bar{1}$, SHG cannot be observed, as this is only apparent when a compound crystallizes in a non-centrosymmetric space group, or if surface effects or defects are dominant, both of which is not the case here. However, amorphous samples of **1**, which are produced by rapid precipitation of the material, display the typical WLG ranging from 450 to 700 nm upon excitation with a 980 nm CW-laser (Supplementary Figs. 16 and 17). The powder X-ray diffraction (PXRD) patterns of samples with different habitus and the broadband emission spectrum obtained from the amorphous sample are shown in Fig. 3.

Materials properties, ink preparation and inkjet printing of compound 1
After the successful synthesis of compound **1**, its structural characterization and determination of the nonlinear optical properties, the next

Fig. 2 | Single-crystal X-ray diffraction results of compound 1. a Molecular structure of compound **1**. **b** Packing of the cluster molecules in the (extended) unit cell. Organic substituents are displayed in wire mode. Heavy atoms are given as thermal displacement ellipsoids with 50% probability. Further images with the full labelling scheme are provided in Supplementary Fig. 15. Selected atomic parameters are given in the text and in Supplementary Table 4.
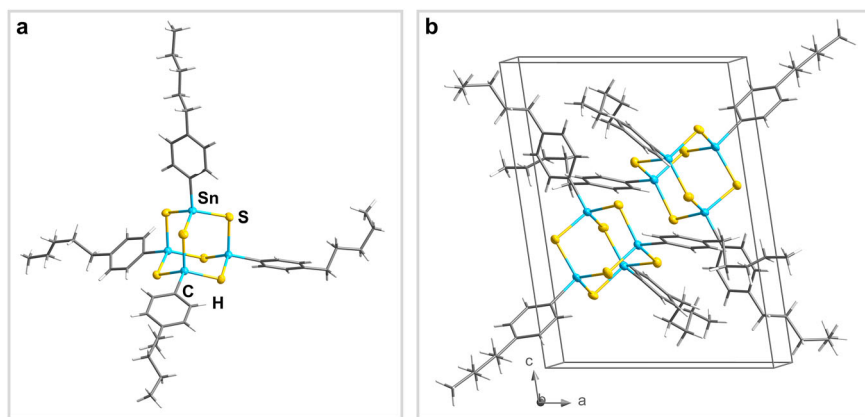

Fig. 3 | Powder X-ray diffraction (PXRD) results and white-light emission of compound 1. a PXRD pattern of compound **1** as crystalline material. **b** PXRD pattern of compound **1** as amorphous material. **c** Phototopic white-light spectrum of the amorphous sample of **1**.
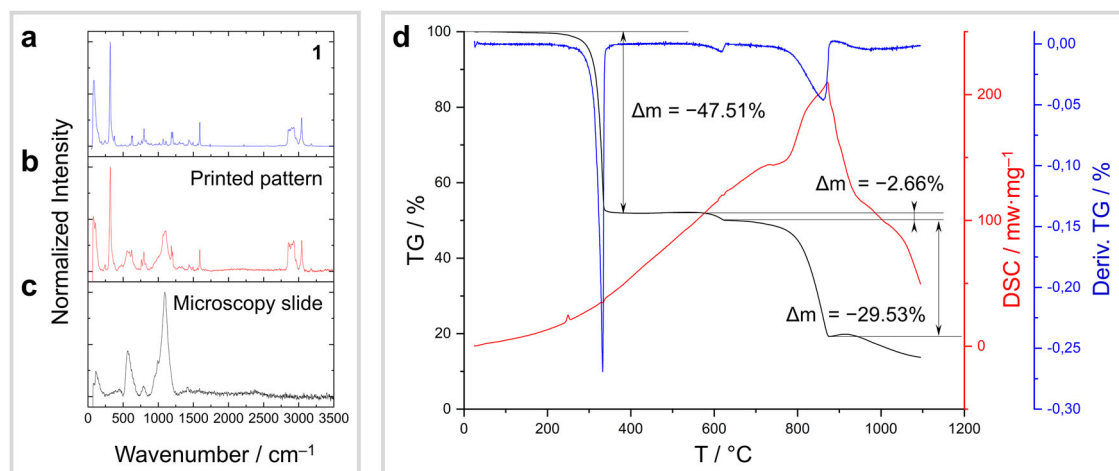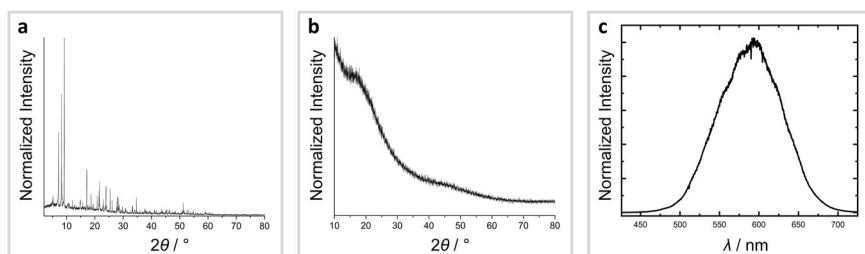

Fig. 4 | Stability analysis after inkjet printing. a Raman spectrum of pristine compound **1** as a reference. **b** Raman spectrum of 5 printed layers of **1** on a microscope slide. **c** Raman spectrum of a pure microscope slide. **d** Thermal analysis of **1** by TGA (black line, derivative in blue) and DSC (red line).

steps were to check the compound's thermal stability, to test the properties of its solutions, and to prepare a printable ink. According to thermogravimetric analysis (TGA) and differential scanning calorimetry (DSC, see Fig. 4, Supplementary Figs. 18–20, and Supplementary Note 1) compound **1** does not decompose below 248 °C, which indicates that its thermal stability is sufficiently high to withstand the operating temperature of the print head. Furthermore, the stability towards different solvents was investigated, indicating that **1** is stable against common organic solvents, such as anisole, toluene, and aqueous solutions like diluted hydrochloric acid or ammonia (see Supplementary Figs. 21–24 and Supplementary Table 5). The organic decoration of compound **1** affects its solubility in organic solvents in an expected way. The solubilities of **1** in toluene and THF are about a factor of 20 higher than that of compound **A**. The solubility in other solvents is also significantly

increased as compared to the solubility of **A** (see Supplementary Table 5). Notably, by mixing **1** with water and surfactants a stable suspension is obtained, as verified by dynamic light scattering (DLS; see Supplementary Fig. 25, Supplementary Table 6, and Supplementary Note 2). As mentioned above, surface tension and viscosity of the inks are important parameters for inkjet printing. To achieve drop formation at the nozzles of the Dimatix DMP-2850 printer, a surface tension of 28–33 mN m^{-1} and a viscosity of 1.0–1.2 mPa s are required. Optimization of the spot size and homogeneity can be achieved by using another type of printer, the Super Inkjet Printer. This device allows for a much better control of the drop size, which can be between 0.1 femtoliters and 10 picoliters. Here, the required viscosity range is 0.5–1.0 mPa s. We explored how the surface tension and viscosity would be affected by different concentrations of compound **1** in toluene, anisole, and chlorobenzene. The pure
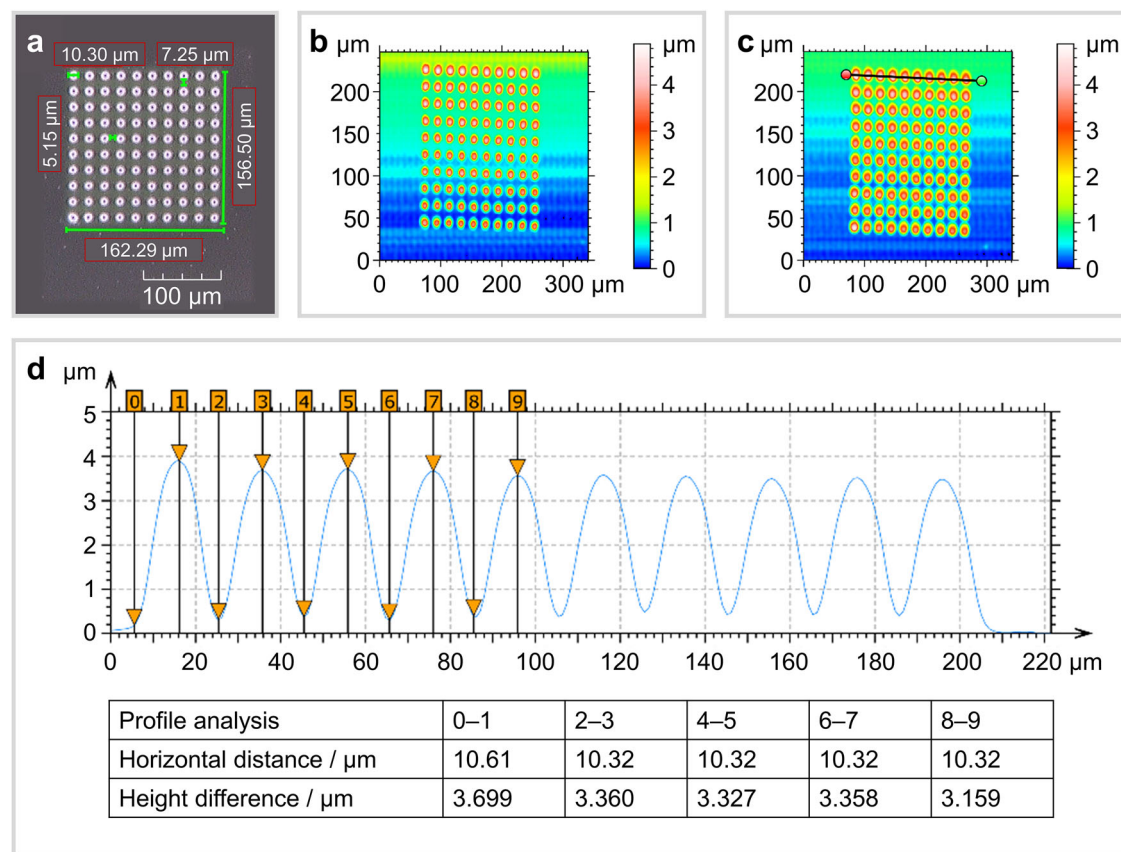
Fig. 5 | Printed patterns of compound 1 in anisole (150 mg mL⁻¹) on glass.
a Microscope image of printed pattern at 300 ms holding time with a 5 μm pitch between the dots. **b** Morphology analysis of the pattern printed at 300 ms holding time. **c** Morphology analysis of the pattern printed at 600 ms holding time, with the line indicating the cross section used for the profile analysis. **d** Profile analysis from the morphology measurement of the pattern printed at 600 ms holding time.

solvents possess surface tensions of 28.5 mN m⁻¹, 34.7l mN m⁻¹, and 33.6 mN m⁻¹, respectively, and a viscosity of 0.480 mPa s, 1.4 mPa s, and 0.753 mPa s, respectively, at 25 °C (see Supplementary Table 7). When the compound was dissolved in an organic solvent, the viscosity was found to increase. The opposite effect was observed with regard to surface tension: dissolving 1 in toluene or chlorobenzene reduced the surface tension of the liquids. To increase the concentration of the cluster in the solvent, this was driven to an extent at which the surface tension reached the lowest possible value suitable for printing. Initial experiments with a toluene-based ink indicated that the ink's viscosity is reduced when being in motion, which is also known as shear thinning, which is generally beneficial for inkjet printing (see Supplementary Figs. 26 and 27). However, the sensitivity on shear thinning and the decrease in surface tension at increased cluster concentration in toluene are disadvantages for stable printing conditions (waveform, temperature, partitioning of particle loading in solvent and surfactant). Thus, this approach was not pursued further for ink preparation. However, it was found that the surface tension of an anisole-based liquid decreases less notably upon addition of 1. Overall, anisole was found to be the most promising basis for a cluster-based ink, with respect to its high boiling temperature as well as a suitable surface tension and viscosity, meeting the requirements of the used printers. It is also the least hazardous solvent, which makes it a good candidate for our purpose. For probing the stability of the cluster compound during printing, a pattern comprising 10 × 10 dots were printed from an anisole-based ink containing 150 mg mL⁻¹ of compound 1 on a microscope slide using a Dimatix DMP-2850 instrument. Each 50–60 μm dot was printed at a distance of 14–30 μm from the next dot, and contained 0.375 ng of 1 per layer, as calculated from the concentration of the ink and the drop size of 2.5 pl produced by the printing head. Patterns comprising 1–5 layers were printed, of which the 5-layer

print contains sufficient material for a Raman-spectroscopic analysis (Fig. 4).

Figure 4 shows the Raman spectra before (see Fig. 4a) and after (see Fig. 4b) the printing process. The spectrum shown in Fig. 4b was recorded after the 5-layer printing of 1 on a microscope slide. Figure 4a, c shows spectra of 1 and the clean microscope slide for reference, respectively. The latter causes the broad signals in the ranges 500–750 cm⁻¹ and 1000–1250 cm⁻¹ in the printed pattern, which otherwise features the Raman fingerprint of 1, clearly indicating that 1 remained perfectly intact under the printing conditions, without being affected by the operating temperatures of the print head (vide supra). The printed patterns were analyzed by a nano-point scanner, which provides detailed insight into the morphology of the surface (see Supplementary Note 3). Supplementary Fig. 28 demonstrates the results of the 1-layer to 5-layer patterns. A profile analysis shows that the first dots of each new line are slightly higher than the following spots, which is due to variability in the volume of the discharged ink reservoir. To minimize the spot size and decrease the distance between dots, the more precise Super Inkjet Printer (SIJ Technology Inc.) was used. This printer ejects ink drops by usage of an electric field which is applied for a specific time span (holding time). With this single-nozzle electro-hydrodynamic printer, a 10 × 10 pattern of dots was printed. The results are illustrated in Fig. 5. The deposition of 1 with holding times of 300 ms led to a well-structured pattern of dots with 10 μm width and 3.2 to 3.7 μm height, printed in a distance of 5 μm (Fig. 5a, b). Larger holding times resulted in higher amounts of deposited material, and eventually an overlap of printed dots at holding times of 1000 ms (see Supplementary Figs. 29 and 30). The deposition of 1 with holding times of 600 ms led to a well-structured pattern without the overlap of dots (Fig. 5c). The resulting spots were approximately 20 μm wide and 3.2 to 3.7 μm tall, with a distance of 5 μm. This serves as an excellent compromise between high amounts of deposited material and the
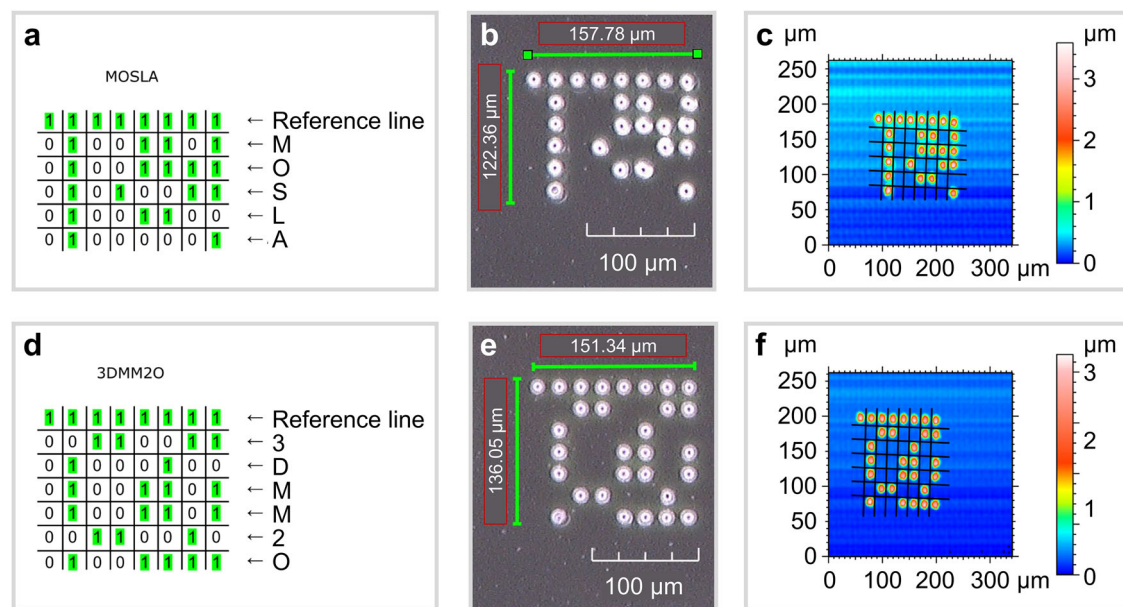
Fig. 6 | Printed cluster-based bit strings. a Calculated binary sequence of "MOSLA" (0 ≙ blank; 1 ≙ compound **1**). **b** Microscope image of the printed pattern of "MOSLA". **c** Morphology analysis of the printed pattern of "MOSLA" with overlaid grid. **d** Calculated binary sequence of "3DMM2O" (0 ≙ blank; 1 ≙ compound **1**). **e** Microscope image of the printed pattern of "3DMM2O". **f** Morphology analysis of the printed pattern of "3DMM2O" with overlaid grid.

still clear separation of printed spots (Fig. 5d). With the same settings, binary sequences of two words were printed (Fig. 6a, d), which represent the acronyms of the projects underlying this study, "MOSLA" (for "Molekulare Speicher zur Langzeit-Archivierung") and "3DMM2O" (for "3D Matter Made to Order"). In these coatings, the value "0" is assigned to a blank data point, while a spot of compound **1** is assigned to the value of "1". The first line represents a reference line for a clearer view, where each data point is "1". The following lines represent the conversion of "MOSLA" and "3DMM2O" into a binary code with 8 data points per character. For "MOSLA", a total of 40 data points were printed in an area of 158×122 μm. For "3DMM2O" this procedure produced a total of 48 data points in an area of 151×136 μm. With the ability of printing **1** in a homogenous pattern, a theoretically possible data density can be approximated for a data storage medium in which two different types of adamantane-type clusters, with slightly differing non-linear optical properties for the read-out, are assigned to the values 0 and 1. One data point is one bit. The assumption for the data density relies on the fact that the Super Inkjet Printer can print 8 data points in approximately 160 μm. In one inch, ~1270 data points can be deposited, which leads to a linear density of ~1270 bit inch^{-1} or an area data density of ~0.19 MB inch^{-2}. In a concept where three different adamantane-type clusters (one exhibiting SHG, and two exhibiting WLG with slightly different λ_{max}) beside one blank character are used, a quaternary cluster-based code would be achieved, which leads to a correspondingly higher data density. Future work will address this next step.

Conclusion

We synthesized an organotetrel chalcogenide adamantane-type cluster compound, $[\{(4\text{-}n\text{-pentyl-phenyl})Sn\}_4S_6]$ (**1**), which is obtained either as a crystalline solid, or as an amorphous molecular material with extreme nonlinear optical properties. Owing to its tailored organic functionalization, it shows superior solubility in organic solvents as compared to previously known analogous clusters. Upon determination of the right carrier solvent for printing, we succeeded in preparing and optimizing an ink and print the cluster material onto a glass substrate with fine spot sizes and high material depositions. The material's nature remained unaffected during the printing process. Two binary sequences, deliberately encrypting the words "MOSLA" and "3DMM2O", were successfully printed to highlight the potential of such clusters as an optical data storage medium. In addition, the

material's superior thermal stability offers the perspective of using it for long-term data storage. These initial studies open the pathway to designing more cluster-based inks to maximize possible data densities.

Methods

General methods

All synthetic steps were performed, if not otherwise specified, under exclusion of water and air by using standard Schlenk techniques. THF, toluene, acetonitrile, and 2-propanol (isopropyl alcohol) were purchased in technical purity. THF was dried over KOH, separated from KOH, dried over potassium and benzophenone for 24 h, distilled, and stored under argon over 4 Å molecular sieves. Toluene was dried over CaCl$_2$, distilled, and stored under argon over 4 Å molecular sieves. Acetonitrile was dried over NaH, distilled, and stored under argon over 3 Å molecular sieves. 2-Propanol was distilled under reduced pressure (1×10^{-3} mbar) and stored under air. THF-d$_8$ (>99.5%, Sigma-Aldrich), CDCl$_3$ (Eurisotop, 99.8%) and C$_6$D$_6$ (Eurisotop, 99.5%) were distilled prior to use and stored under argon over 4 Å molecular sieves. 4-n-Pentylphenyl bromide (BLDpharm, 99.9%), Mg (Sigma-Aldrich, 99.5%), SnCl$_4$ (Sigma-Aldrich, 98.0%), anisole (Fluka Analytical, 99.0%), 1,2-dibromoethane (VWR, >99%), mesitylene (Thermo scientific, >98%), dichloromethane (VWR, >99.5%), SDS (PanReac AppliChem, 99.0%), Triton X-100 (Acros Organics), TMDD (BLDpharm, 97.62%), ammonia (ROTH Ph. Eur., 25%), and HCl (FLUKA p.a., 36%) were used without further purification. (Me$_3$Si)$_2$S was prepared according to literature procedures[34].

Synthesis of tetra(4-n-pentyl-phenyl)stannane, (4-n-pentyl-phenyl)$_4$Sn (I)

Mg (15.13 g, 617 mmol, 8 equiv.) was suspended in THF (500 mL) and 1,2-dibromoethane (2 mL) was added and the mixture stirred at room temperature for 30 min. Next, 4-n-pentyl-phenyl bromide (72 g, 317 mmol, 4.1 equiv.) was added over 45 min. The reaction solution was refluxed at 80 °C for 3.5 h. The dark grey suspension was filtered into a dropping funnel and added dropwise to a toluene solution (500 mL) of SnCl$_4$ (9 mL, 2.23 g mL^{-1}, 78 mmol, 1 equiv.) over 75 min. After addition, the solution was refluxed at 100 °C for 3 h. The resulting slightly yellow solution with white precipitate was quenched with 150 mL of distilled water, and the suspension was filtered via a glass frit to remove most of the solid and again by gravity filtration

for the remaining finely dispersed solid. The clear phases were separated, and the organic phase was evaporated under reduced pressure (1×10^{-3} mbar) to give an oily residue. A small volume of toluene (100 mL) was added followed by acetonitrile (500 mL). The solid that formed was filtered off, and again dissolved in toluene and treated with acetonitrile. The recrystallized solid was filtered and dried under reduced pressure (1×10^{-3} mbar) for three days to give a white sticky powder. Single crystals of (4-*n*-pentyl-phenyl)$_4$Sn (**I**) suitable for X-ray crystallography were grown by dissolving the solid in 10 mL of toluene, layering it with acetonitrile and storing it at $-40\,°C$. The crystals were grown at the liquid-gas interface.

Yield: 37.34 g (68%, 53 mmol, $C_{44}H_{60}Sn$, 707.67 g mol^{-1}). **^{1}H NMR** (300.19 MHz, CDCl$_3$, δ): 7.51 ppm (d, 8H, ^3J(3H-2H) = 7.5 Hz, ^3J(^{1}H-^{119}Sn) = 46.8 Hz, ^3J(^{1}H-^{117}Sn) = 156.36 Hz, H3), 7.2 ppm (d, 8H, ^3J(3H-2H) = 7.5 Hz, ^4J(^{1}H-^{119}Sn) = 58.7 Hz, ^4J(^{1}H-^{117}Sn) = 157.1 Hz, H2), 2.60 ppm (t, 8H, H5), 1.62 ppm (*quintet*, 8H, H6), 1.42-1.20 ppm (m, 16H, H7/H8), 0.89 ppm (t, 9H, H9). **^{13}C{^{1}H} NMR** (75.49 MHz, CDCl$_3$, δ): 143.8 ppm (^4J(^{13}C-$^{119/117}$Sn) = 11.2 Hz, C4), 137.3 ppm (^2J(^{13}C-$^{119/117}$Sn) = 38.5 Hz, C2), 135.0 ppm (C1), 128.8 ppm (^3J(^{13}C-$^{119/117}$Sn) = 52.1 Hz, C3), 36.2 ppm (C5), 31.8 ppm (C6), 31.3 ppm (C7), 22.7 ppm (C8), 14.2 ppm (C9). **^{119}Sn{^{1}H} NMR** (111.97 MHz, CDCl$_3$, δ): -125.9 ppm. **IR** (ATR): $\tilde{v}$ = 3058 (w), 3007 (w), 2955 (m), 2924 (s), 2854 (m), 1909 (w), 1808 (w), 1590 (w), 1553 (w), 1493 (w), 1460 (m), 1392 (m), 1262 (w), 1186 (m), 1108 (w), 1071 (m), 1015 (w), 822 (m), 795 (m), 727 (w), 620 (w), 591 (w), 521 (m), 474 (w), 435 cm^{-1} (w).

Synthesis of trichloro(4-*n*-pentyl-phenyl)stannane, (4-*n*-pentyl-phenyl)SnCl$_3$ (II)

(4-*n*-pentyl-phenyl)$_4$Sn (2.02 g, 2.85 mmol, 1 equiv.) was treated with SnCl$_4$ (1 mL, 2.23 g mL^{-1}, 8.56 mmol, 3 equiv.) in a Schlenk flask. After a few minutes the slurry turned dark grey. Subsequent heating at 150 °C for 3 h, followed by distillation under reduced pressure (1×10^{-3} mbar, 104 °C) yielded (4-*n*-pentyl-phenyl)SnCl$_3$ (**II**) as a colorless liquid. Yield: 3.13 g (74%, 8.42 mmol, $C_{11}H_{15}SnCl_3$, 372.30 g mol^{-1}). **B.p.**: 104 °C (1×10^{-3} mbar). **^{1}H NMR** (300.19 MHz, C$_6$D$_6$, δ): 7.16 ppm (d, 2H, ^3J(3H-2H) = 8.0 Hz, ^4J(^{1}H-^{119}Sn) = 116.6 Hz, ^4J(^{1}H-^{117}Sn) = 161.0 Hz, H3), 6.81 ppm (d, 2H, ^3J(3H-2H) = 8.0 Hz, ^3J(^{1}H-^{119}Sn) = 48.6 Hz, ^3J(^{1}H-^{117}Sn) = 159.8 Hz, H2), 2.26 ppm (t, 2H, H5), 1.43-1.04 ppm (m, 6H, H6/H7/H8), 0.87 ppm (t, 3H, H9). **^{13}C{^{1}H} NMR** (75.49 MHz, C$_6$D$_6$, δ): 148.6 ppm (^4J(^{13}C-$^{119/117}$Sn) = 25.4 Hz, C4), 134.0 ppm (^2J(^{13}C-$^{119/117}$Sn) = 79.0 Hz, ^2J(^{13}C-$^{119/117}$Sn) = 82.4 Hz, C2), 132.8 ppm (C1), 130.5 ppm (^3J(^{13}C-$^{119/117}$Sn) = 124.2 Hz, ^3J(^{13}C-$^{119/117}$Sn) = 130.2 Hz, C3), 36.0 ppm (^5J(^{13}C-$^{119/117}$Sn) = 12.3 Hz, C5), 31.6 ppm (C6), 31.0 ppm (C7), 22.8 ppm (C8), 14.2 ppm (C9). **^{119}Sn{^{1}H} NMR** (111.95 MHz, C$_6$D$_6$, δ): -56.4 ppm.

Synthesis of 1,3,5,7-tetra(4-*n*-pentyl-phenyl)-2,4,6,8,9,10-hexathia-1,3,5,7-tetrastanna-adamantane, [{(4-*n*-pentyl-phenyl)Sn}$_4$S$_6$] (1)

(4-*n*-pentyl-phenyl)SnCl$_3$ (11.12 g, 29 mmol, 4 equiv.) was dissolved in 80 mL of toluene in a Schlenk flask and (Me$_3$Si)$_2$S (9.44 mL, 0.846 mg mL^{-1}, 44 mmol, 6 equiv.) was added over 20 min. The reaction solution was stirred at room temperature for 4 days. After removal of the solvent under reduced pressure (1×10^{-3} mbar), the resulting orange oil was dissolved in 12 mL of toluene, and 250 mL of acetonitrile were added. Subsequent storage at $-40\,°C$ for 24 h led to the formation of a colorless precipitate. The solid was filtered, washed three times with 10 mL of cold acetonitrile ($-30\,°C$), and dried under reduced pressure (1×10^{-3} mbar). [{(4-*n*-pentyl-phenyl)Sn}$_4$S$_6$] (**1**) was obtained as a colorless powdery solid. Single crystals were grown by dissolving the as-prepared material in 2-propanol with subsequent slow evaporation of the solvent over several days.

Yield: 8.62 g (92%, 1.74 mmol, $C_{44}H_{60}S_6Sn_4$, 1256.16 g·mol^{-1}). **M.p.**: 90 °C. **^{1}H NMR** (300.19 MHz, CDCl$_3$, δ): 7.59 ppm (d, 2H, ^3J(3H-2H) = 8.0 Hz, ^4J(^{1}H-^{119}Sn) = 83.5 Hz, H3), 7.32 ppm (d, 2H, ^3J(3H-2H) = 8.0 Hz, ^3J(^{1}H-$^{119/117}$Sn) = 29.2 Hz, H2), 2.63 ppm (t, 2H, H5), 1.63 ppm (*quintet*, 2H, H6), 1.42-1.21 ppm (m, 2H, H7/H8), 0.90 (t, 3H, H9). **^{13}C{^{1}H} NMR** (75.49 MHz, CDCl$_3$, δ): 146.7 ppm (C4), 138.8 ppm (C1), 133.9 ppm (C2), 129.8 ppm (C3), 36.2 ppm (C5), 31.6 ppm (C6), 31.1 ppm (C7), 22.7 ppm (C8), 14.1 ppm (C9). **^{119}Sn{^{1}H} NMR** (111.95 MHz, THF-d$_8$, δ): 80.8 ppm. **^{119}Sn{^{1}H} NMR** (111.97 MHz, C$_6$D$_6$, δ): 85.5 ppm. **^{119}Sn{^{1}H} NMR** (111.97 MHz, CDCl$_3$, δ): 84.8 ppm. **IR** (ATR): $\tilde{v}$ = 3033 (w), 2922 (s), 2854 (s), 1901 (w), 1793 (w), 1586 (w), 1553 (w), 1491 (w), 1454 (m), 1388 (m). 1184 (m), 1110 (w), 1065(m), 1009 (m), 968 (w), 935 (w), 824 (m), 787 (s), 723 (m), 620 (w), 589 (w), 515 (s), 474 (w). **Raman** (laser: 532 nm, accumulation time: 10 s, 297 K): $\tilde{v}$ = 3177 (w), 3039 (m), 2930 (m), 2897 (m), 2874 (m), 2852 (m), 2219 (w), 1738 (w), 1591 (m), 1558 (w), 1493 (w), 1437 (w), 1398 (w), 1301 (w), 1238 (w), 1205 (w), 1190 (w), 1109 (w), 1071 (w), 1014 (w), 898 (w), 825 (w), 798 (w), 762 (w), 715 (w), 632 (w), 622 (w), 593 (w), 473 (w), 375 (w), 314 (s), 240 (w), 188 (w), 150 (w), 83 (s).

Evaluation of solution and solubility behavior of 1

For the evaluation of the stability and solubility behavior, 10 mg of **1** were filled in a 10 mL glass vial with a magnetic stirring bar. After addition of 5 mL of the solvent (anisole, 1,4-dioxane, mesitylene, dichloromethane, toluene, THF, aqueous HCl, aqueous NH$_3$), the solution or suspension was stirred for 24 h. In case of the solutions, the solvent was evaporated off, and a ^{1}H or ^{13}C{^{1}H} NMR spectrum in C$_6$D$_6$ or CDCl$_3$, respectively, was recorded from the residue. The suspensions were filtered, and a ^{1}H or ^{13}C{^{1}H} NMR spectrum in C$_6$D$_6$ or CDCl$_3$, respectively, was recorded from the residue.

Ink preparation and characterization

To obtain a printable fluid, 650–750 mg of **1** were filled in a 10 mL glass vial with a magnetic stirring bar. After adding 5 mL of anisole, the resulting mixture was stirred for 3 h until the solid completely dissolved. For water-based suspensions, 10 mg of **1** were filled in a 10 mL glass vial with a magnetic stirring bar. The surfactant solutions of SDS and TMDD were prepared in a separate 10 mL glass vial. The glass vial was filled with 115 mg of SDS or 15 mg of TMDD, and a magnetic stirring bar and 10 mL of distilled water were added. The resulting mixture was stirred for 1 h to completely dissolve the surfactant. In the next step, the surfactant solution was added to the vial filled with **1**, and stirred for 15 min. The surface tension was measured on a DSA 100 device from Krüss via the pendant drop method. The viscosity and shear viscosity measurements were performed using a KINEXUS lab+ from Malvern Panalytical equipped with a cone-plate. Viscosity was measured under shear conditions using a rotational viscometer equipped with a cone plate.

NMR spectroscopy

^{1}H, ^{13}C and ^{119}Sn NMR spectra were recorded on a Bruker AV II 300 MHz or AV III HD 300 MHz. The chemical shifts were referenced to the deuterated solvent signals of CDCl$_3$ = 7.260 ppm (^{1}H)/ 77.160 ppm (^{13}C); C$_6$D$_6$ = 7.160 ppm (^{1}H)/ 128.060 ppm (^{13}C); THF-d$_8$ = 3.58 ppm (^{1}H)/ 67.57 ppm (^{13}C). The raw data was processed with MestReNova 14.2.0-26256.

Powder X-ray diffraction (PXRD)

Powder-XRD data were collected on a STOE STADI MP equipped with a Cu-Kα radiation source and a Mythen detector system at room temperature in transmission mode. The data was processed by using WinXPOW.

Micro-X-ray fluorescence (μ-XRF) spectroscopy

μ-XRF data were recorded on a Bruker M4 Tornado, equipped with a Rh-target X-ray tube and a silicon drift detector. The emitted fluorescence photons were detected with an acquisition time of 240 s.

Dynamic light scattering (DLS)

DLS samples were measured on a DynaPro NanoStar from Wyatt Technology. Collected data was analyzed via the Dynals algorithm using the program DYNAMICS 7.9.0.5. The samples were prepared in disposable cuvettes under air, and measured at 25 °C. Before measuring the samples, they were filtered via a sterile 0.22 μm PVDF single use syringe filter.

TGA/DSC
Thermal properties were investigated using a Netzsch STA 409 CD. Raw data were processed using OriginPro23 10.0.0.154.

Inkjet printing
Printing experiments were performed on a Dimatix DMP-2850 (Fujifilm) with disposable cartridges including 12–16 nozzle dispenser heads or on a Super Inkjet Printer (SIJ Technology Inc.). The Dimatix DMP-2850 works with fluid viscosities of 10 to 12 mPa s and a surface tension of 28 to 33 mN m^{-1}. The substrate was cleaned with a cloth before printing. The droplets produced during successful printing were stable and the printout appears uniform and free of noteworthy errors. During determining the optimal printing parameters, we noticed instabilities in droplet formation, which were adjusted accordingly to improve the results. A frequency sweep showed that jetting frequencies around 10 kHz are sufficient to form droplets. Owing to the favorable solvent properties of anisole, possessing a viscosity of ~0.99 mPa s and a surface tension of ~34 mN/m, which are very suitable for inkjet printheads, no further optimization was required. Very minor coffee ring effects were initially observed for larger dots, but not at all for smaller dots. No defects were found after the dots had dried.

Surface morphology analysis
To analyze the surface morphology of the printed patterns, a Hirox Nano Point Scanner was used with a sensor frequency of 1000 Hz, a scanning speed of 1000 μm s^{-1}, and a sensor range of 150 μm.

Raman spectroscopy
Raman spectra were recorded on a Renishaw inVia Raman confocal microscope equipped with a 532 nm laser. Raw data were baseline corrected, smoothed with the Savitzky-Golay filter[34], and normalized to 1. Data were processed with OriginPro23 10.0.0.154.

IR spectroscopy
Infrared spectra were recorded on a Bruker Alpha II or Bruker Tensor37. Raw data was baseline-corrected, smoothed with the Savitzky-Golay filter[35], and normalized to 1. Data were processed with OriginPro23 10.0.0.154.

X-ray crystallography
X-ray diffractometry was done with a Mo-Kα radiation source at 100 K, using a Bruker D8 Quest or a Stoe StadiVari diffractometer. Reflection data were processed with X-Area 2.1. The structures were solved by dual space methods in SHELXT[36] and refined by full matrix-least-squares refinement against F^2 in SHELXL[37], using the Olex2[38] user interface.

Nonlinear optical measurements
For measuring the nonlinear optical response an in-house build setup was used. The setup uses an 980 nm CW-laser for excitation. The laser is focused onto the samples using a f = 10 cm lens. Typical excitation power is 353 mW resulting in an excitation density of 1100 W cm^2 at the sample position. The sample is kept in a vacuum chamber under static vacuum of ~1×10^{-4} mbar mounted on a *xyz*-translational stage. The light emitted by the sample is relayed and focused onto a compact spectrometer (OceanOptics HR2000). For blocking residual excitation light a bandpass filter (Schott KG2) is placed in front of the spectrometer. To account for spectral response and transmission of the filter, the system response is corrected using a standard tungsten halogen lamp. A sketch of the setup is shown in Supplementary Fig. 16.

Data availability
All data generated or analyzed during this study are included in this published article and its supplementary information files. The structures of compound **I** and **1** were determined by single-crystal X-ray diffraction. The X-ray crystallographic coordinates for structures reported in this Article have been deposited at the Cambridge Crystallographic Data Centre (CCDC), under deposition numbers CCDC-2425710 (**I**) and CCDC-2425711 (**1**). These data can be obtained free of charge from The Cambridge Crystallographic Data Centre via www.ccdc.cam.ac.uk/data_request/cif. The CIFs of compounds **I** and **1** are supplied as Supplementary Data 1 and Supplementary Data 2, respectively.

References
1. Piatti, E. et al. Charge transport mechanisms in inkjet-printed thin-film transistors based on two-dimensional materials. *Nat. Electron* **4**, 893–905 (2021).
2. Singh, M., Haverinen, H. M., Dhagat, P. & Jabbour, G. E. Inkjet printing—process and its applications. *Adv. Mater.* **22**, 673–685 (2010).
3. Wijshoff, H. The dynamics of the piezo inkjet printhead operation. *Phys. Rep.* **491**, 77–177 (2010).
4. Wang, Y., Yi, C., Tian, W., Liu, F. & Cheng, G. J. Free-space direct nanoscale 3D printing of metals and alloys enabled by two-photon decomposition and ultrafast optical trapping. *Nat. Mater.* **23**, 1645–1653 (2024).
5. Yang, L. et al. Laser printed microelectronics. *Nat. Commun.* **14**, 1103 (2023).
6. Hoath, S. D. *Fundamentals of Inkjet Printing: The Science of Inkjet and Droplets*. 1st ed. (Wiley-VCH, Weinheim, 2016).
7. Park, J.-U. et al. High-resolution electrohydrodynamic jet printing. *Nat. Mater.* **6**, 782–789 (2007).
8. Teng, K. F. & Vest, R. W. Metallization of solar cells with ink jet printing and silver metallo-organic inks. *IEEE Trans. Compon. Hybrids Manuf. Technol.* **11**, 291–297 (1988).
9. Rozenberg, G. G., Bresler, E., Speakman, S. P., Jeynes, C. & Steinke, J. H. G. Patterned low temperature copper-rich deposits using inkjet printing. *Appl. Phys. Lett.* **81**, 5249–5251 (2002).
10. Goldie, D. M., Hourd, A. C., Harvie, M. R., Thomson, J. & Abdolvand, A. Scatter-limited conduction in printed platinum nanofilms. *J. Mater. Sci.* **50**, 1169–1174 (2015).
11. Hou, Y. et al. Highly emissive perylene diimide-based metallacages and their host-guest chemistry for information encryption. *J. Am. Chem. Soc.* **142**, 18763–18768 (2020).
12. Grant, T. D. et al. Inkjet printing of high-concentration particle-free platinum inks. *Mater. Des.* **214**, 110377 (2022).
13. Schoner, C. et al. Particle-free gold metal–organic decomposition ink for inkjet printing of gold structures. *Thin Solid Films* **531**, 147–151 (2013).
14. Cirelli, M. et al. Printing "smart" inks of redox-responsive organometallic polymers on microelectrode arrays for molecular sensing. *ACS Appl. Mater. Interfaces* **11**, 37060–37068 (2019).
15. Smith, P. J., Shin, D.-Y., Stringer, J. E., Derby, B. & Reis, N. Direct ink-jet printing and low temperature conversion of conductive silver patterns. *J. Mater. Sci.* **41**, 4153–4158 (2006).
16. Zhao, Y. et al. A novel and facile route of ink-jet printing to thin film SnO$_2$ anode for rechargeable lithium ion batteries. *Electrochim. Acta* **51**, 2639–2645 (2006).
17. Yoboue, P. et al. When organometallic chemistry and metal oxide nanoparticles meet optimized silicon-based gas sensor. *Mater. Res. Soc. Symp. Proc.* **1253**, K05–K18 (2010).
18. Qin, Y., Alam, A. U., Howlader, M. M. R., Hu, N.-X. & Deen, M. J. Inkjet printing of a highly loaded palladium ink for integrated, low-cost pH sensors. *Adv. Funct. Mater.* **26**, 4923–4933 (2016).
19. Hamacher, S., Bachmann, B. & Yakushenko, A. Development of a gold nanoparticle conductive ink with a relatively low sintering temperature. *TechConnect Briefs* **4**, 141–144 (2017).
20. Grouchko, M., Kamyshny, A. & Magdassi, S. Formation of air-stable copper–silver core–shell nanoparticles for inkjet printing. *J. Mater. Chem.* **19**, 3057 (2009).

21. Hu, H. et al. Inkjet-printed bipolar resistive switching device based on Ag/ZnO/Au structure. *Appl. Phys. Lett.* **119**, 112103 (2021).

22. Sun, J., Sun, R., Jia, P., Ma, M. & Song, Y. Fabricating flexible conductive structures by printing techniques and printable conductive materials. *J. Mater. Chem.* **C 10**, 9441–9464 (2022).

23. Haverinen, H. M., Myllylä, R. A. & Jabbour, G. E. Inkjet printing of light emitting quantum dots. *Appl. Phys. Lett.* **94**, 073108 (2009).

24. Xuan, T., Shi, S., Wang, L., Kuo, H.-C. & Xie, R.-J. Inkjet-printed quantum dot color conversion films for high-resolution and full-color micro light-emitting diode displays. *J. Phys. Chem. Lett.* **11**, 5184–5191 (2020).

25. Moon, H., Lee, C., Lee, W., Kim, J. & Chae, H. Stability of quantum dots, quantum dot films, and quantum dot light-emitting diodes for display applications. *Adv. Mater.* **31**, e1804294 (2019).

26. Rosemann, N. W. et al. A highly efficient directional molecular white-light emitter driven by a continuous-wave laser diode. *Science* **352**, 1301–1304 (2016).

27. Rosemann, N. W., Eußner, J. P., Dornsiepen, E., Chatterjee, S. & Dehnen, S. Organotetrel chalcogenide clusters: between strong second-harmonic and white-light continuum generation. *J. Am. Chem. Soc.* **138**, 16224–16227 (2016).

28. Haust, J. et al. White light generating molecular materials: correlation between the amorphous/crystalline structure and nonlinear optical properties. *ChemPhotoChem* **6**, e202200071 (2022).

29. Hanau, K. et al. Towards understanding the reactivity and optical properties of organosilicon sulfide clusters. *Angew. Chem. Int. Ed.* **60**, 1176–1186 (2021).

30. Schwan, S. et al. Insights into molecular cluster materials with adamantane-like core structures by considering dimer interactions. *J. Comput. Chem.* **44**, 843–856 (2023).

31. Dornsiepen, E., Dobener, F., Chatterjee, S. & Dehnen, S. Controlling the white-light generation of $(RSn)_4E_6$: effects of substituent and chalcogenide variation. *Angew. Chem. Int. Ed.* **58**, 17041–17046 (2019).

32. Dornsiepen, E., Eußner, J. P., Rosemann, N. W., Chatterjee, S. & Dehnen, S. Syntheses and properties of gold-organotin sulfide clusters. *Inorg. Chem.* **56**, 11326–11335 (2017).

33. Pöhlker, C., Schellenberg, I., Pöttgen, R. & Dehnen, S. Synthesis and reactivity of ferrocenyl functionalized Sn/S Cages. *Chem. Commun.* **46**, 2605–2607 (2010).

34. So, J.-H. & Boudjouk, P. Convenient syntheses of hexamethyldisilathiane and tetramethyldisilathiane. *Synthesis* **4**, 306–307 (1989).

35. Savitzky, A. & Golay, M. J. E. Smoothing and differentiation of data by simplified least squares procedures. *Anal. Chem.* **36**, 1627–1639 (1964).

36. Sheldrick, G. M. SHELXT - Integrated space-group and crystal-structure determination. *Acta Crystallogr. Sect. A* **71**, 3–8 (2015).

37. Sheldrick, G. M. Crystal structure refinement with SHELXL. *Acta Crystallogr. Sect. C* **71**, 3–8 (2015).

38. Dolomanov, O. V., Bourhis, L. J., Gildea, R. J., Howard, J. A. K. & Puschmann, H. OLEX2: a complete structure solution, refinement and analysis program. *J. Appl. Crystallogr.* **42**, 339–341 (2009).

Acknowledgements

Author contributions

S. N. and Y. R. L. conceived and performed the synthetic experiments, collected single-crystal X-ray crystallographic data, solved and refined the structures and prepared the samples for further characterization under supervision of S. D. and N. R.; S. N. prepared the inks and planned the print patterns; G. C. M. operated the inkjet devices and the nano point scanner under supervision of J. A.-H.; M. W. and D. H. provided the binary codes; N. W. R. performed the nonlinear optical spectroscopy measurements. All authors co-wrote the paper.

Funding

Competing interests

The authors declare no competing interests.

Additional information

Supplementary information The online version contains supplementary material available at https://doi.org/10.1038/s43246-025-00922-z.

Correspondence and requests for materials should be addressed to Jasmin Aghassi-Hagmann or Stefanie Dehnen.

Peer review information *Communications Material* thanks anonymous reviewers for their contribution to the peer review of this work.

Reprints and permissions information is available at http://www.nature.com/reprints

Publisher's note Springer Nature remains neutral with regard to jurisdictional claims in published maps and institutional affiliations.